JOURNAL OF COMPUTATIONAL PHYSICS 104, 427–443 (1993)

Uniform High-Order Spectral Methods for One- and Two-Dimensional Euler Equations*

WEI CAI

Department of Mathematics, University of North Carolina at Charlotte, Charlotte, North Carolina 28223

AND

CHI-WANG SHU

Division of Applied Mathematics, Brown University, Providence, Rhode Island 02912

Received January 18, 1991; revised April 27, 1992

In this paper we study uniform high-order spectral methods to solve multi-dimensional Euler gas dynamics equations. Uniform high-order spectral approximations with spectral accuracy in smooth regions of solutions are constructed by introducing the idea of the essentially non-oscillatory polynomial (ENO) interpolations into the spectral methods. Based on the new approximations, we propose nonoscillatory spectral methods which possess the properties of both upwinding difference schemes and spectral methods. We present numerical results for inviscid Burgers' equation, various one-dimensional Euler equations including the interactions between a shock wave and density disturbances, Sod's and Lax's, and blast wave problems. Finally, we simulate the interaction between a Mach-3 two-dimensional shock wave and a rotating vortex.

1. INTRODUCTION

Recently, high-order numerical methods have attracted considerable interests for the simulations of flows with shock waves and different scales, especially for turbulent flows affected by shock-wave interactions. Those high-order methods are expected to produce nonoscillatory sharp shock profiles without too much overall numerical diffusion and, at the same time, be able to resolve the small scales of the flow field elsewhere. Recent results with essentially nonoscillatory (ENO) finite difference methods have made considerable progress in this direction [9, 17]. Spectral methods, as high-order global methods, have been very successful in studies of turbulent flows and flow transition problems when the solutions of the fluid problems are smooth. For those problems, spectral methods have been shown to have an accuracy higher than any algebraic order (so called spectral accuracy) [5]. However it remains to show that spectral methods will also be successful in computing flows with shock waves.

In this paper, we continue our previous work [4] in designing essentially nonoscillatory spectral methods for computing the weak solutions of the hyperbolic system of conservation laws

$$\mathbf{u}_t + \mathbf{f}(\mathbf{u})_x + \mathbf{g}(\mathbf{u})_y = 0 \tag{1.1}$$

$$\mathbf{u}(x, y, 0) = \mathbf{u}_0(x, y). \tag{1.2}$$

Here, as usual, $\mathbf{u} = (u_1, ..., u_s)^T$ is a state vector and $\mathbf{f}(\mathbf{u})$, $\mathbf{g}(\mathbf{u})$ are the vector-valued flux functions of s components. The system is assumed to be hyperbolic in the sense that for any real vector $\xi = (\xi_1, \xi_2)$, the matrix $\xi_1(\partial \mathbf{f}/\partial \mathbf{u}) + \xi_2(\partial \mathbf{g}/\partial \mathbf{u})$ always has s real eigenvalues and a complete set of eigenvectors. The solutions to (1.1) usually develop discontinuities in the form of shock waves and contact discontinuities.

In applying spectral methods to problems having discontinuous solutions, a key issue is how to deal with the Gibbs phenomenon caused by the discontinuities of the solutions. The overall accuracy of spectral methods will be, at most, first order everywhere in the presence of Gibbs oscillations. There are various filtering techniques to recover spectral accuracy in the regions away from the discontinuities [8, 14]. On the other hand, one-sided filtering can be used to obtain uniform convergence in the regions close to the

* The first author has been supported by NSF Grants, ASC-9005874 and ASC-9113895, supercomputing grant from the North Carolina Supercomputer Center, and a faculty research grant from UNC Charlotte. The second author was partially supported by NSF grant DMS 88-10150, NASA Langley Grant NAG1-1145, NASA Contract NAS1-18605, and AFORSR 90-0093.

0021-9991/93 $5.00

discontinuities [2]. As another approach to treat the Gibbs oscillations, in [4] we proposed a nonoscillatory spectral approximation to discontinuous solutions by adding piecewise linear functions, such as sawtooth-like functions and step functions, to the conventional Fourier trigonometric or Chebyshev polynomial spaces. Those additional functions are used to resolve the discontinuities in the solutions caused by shock waves and contact discontinuities. The cell-averaged form of (1.1) is used to formulate the numerical schemes, resulting in Godunov-type shock capturing algorithms. The usual reconstruction step between cell averages and point values of the numerical solutions in such schemes can be done efficiently with fast Fourier transformations. However, a common problem with cell-averaged formulation is the costly implementation of the reconstructions in multi-dimensional problems.

In this paper, we adopt the same philosophy as in [4], however, a more robust and sophisticated technique will be introduced. With the new technique, we will be able to achieve global convergence up to any given mth order ($m > 0$) and, meanwhile, retain spectral accuracy in the regions away from the discontinuities. In order to achieve these goals, we incorporate the main idea of the ENO polynomial interpolations [9] into our construction of uniform spectral approximations. We also introduce the idea of upwind differencing from conservative finite difference methods into the design of the spectral schemes. The idea of upwind differencing has proven very successful in capturing shock wave fronts and producing entropy satisfying solutions. By using local Riemann solvers and flux limiters, modern shock capturing finite difference schemes, like TVD schemes [9], MUSCL-type schemes [19], FCT schemes [1], and the more recent ENO schemes [9, 17], produce very satisfactory shock profiles and entropy satisfying solutions. The nonoscillatory spectral approximations proposed in this paper will enable us to bring the upwind idea into the framework of spectral methods. Meanwhile, the spectral schemes will be based directly on the conservation laws (1.1), not its cell-averaged form. Thus, generalization to the multi-dimensional cases will be straightforward.

For the system of conservation laws, in order to achieve sharp shock profile without spurious oscillations, numerical flux operators for the scalar equations are usually applied to the locally defined characteristic variables. Because of this complication, it has been realized that the cost of upwind schemes is much greater than that of the centered difference schemes. Several attempts have been made to eliminate this shortcoming by combining center difference schemes and upwind schemes. In [13], a mixed method of center difference schemes and ENO schemes was studied and, in [6], the authors suggested a type of nonlinear filtering technique to modify the results of the Lax–Wendroff scheme at each time step to produce nonoscillatory TVD solutions. The result in this paper will provide another example of blending the nice properties of both upwind scheme and center difference schemes (in this case, spectral schemes).

This paper is organized as follows: in Section 2, we first briefly review the method proposed in [4], then present the new method of constructing uniform convergent, up to any given mth order ($m > 0$), spectral approximations to discontinuous functions. In Section 3, we study the nonoscillatory spectral methods for scalar conservation laws. Extensions to the system of conservation laws and multi-dimensional problems will be discussed in Section 4. In Section 5, we present numerical experiments for the new methods. First, the uniform convergence and the spectral accuracy of the proposed spectral approximations are tested on discontinuous functions. Then we study the global accuracy of the spectral schemes on a scalar inviscid Burgers' equation and one-dimensional Euler equations which model the interaction of a pure shock wave with density waves. Also we apply the scheme to the standard Sod's and Lax's test problems [16] in order to check the convergence of the spectral schemes with respect to the correct entropy solutions. High-order numerical results will also be presented for solving the interaction between two blast waves [20]. Finally, we apply the spectral schemes to simulate the interactions between a Mach-3 two-dimensional shock wave and rotating vortices.

2. UNIFORM HIGH-ORDER SPECTRAL APPROXIMATIONS

The conventional Fourier spectral space has basis functions $\{e^{ikx}\}_{|k| \leqslant N}$. The Fourier expansions for discontinuous functions converge very slowly. For instance, consider a sawtooth-like function

$$F(x, x_s, A) = A \begin{cases} -x & \text{for } x \leqslant x_s, \\ 2\pi - x & \text{for } x > x_s, \end{cases} \tag{2.1}$$

where x_s is the location of the discontinuity and $A = (F(x_s^+) - F(x_s^-))/2\pi = [F]_{x_s}$ is the jump of $F(x, x_s, A)$ across x_s.

The partial sum of the Fourier expansion of $F(x, x_s, A)$ is

$$F_N(x, x_s, A) = \sum_{|k| \leqslant N} \tilde{f}_k(x_s, A)\, e^{ikx}, \tag{2.2}$$

where

$$\begin{aligned} \tilde{f}_k(x_s, A) &= \frac{1}{2\pi} \int_0^{2\pi} F(x, x_s, A)\, e^{-ikx}\, dx \\ &= A \begin{cases} e^{-ikx_s}/(ik) & \text{for } |k| \geqslant 1, \\ (\pi - x_s) & \text{for } k = 0. \end{cases} \end{aligned} \tag{2.3}$$

From (2.3) we see that the Fourier coefficients $\tilde{f}_k(x_s, A)$ only decay like $O(1/k)$ as $k \to \infty$. As a result, the convergence of (2.2) will be only first order, and moreover, the Gibbs oscillations near x_s will be in the order of $O(1)$. In order to get rid of the Gibbs oscillations, in [4] we proposed a technique to construct essentially nonoscillatory spectral approximations, which we review below.

Let $u(x)$ be a piecewise C^∞ periodic function with a jump discontinuity at x_s with jump $[u]_{x_s}$ and, if $u_N(x)$ is its finite Fourier expansion, then the nonoscillatory spectral approximation is defined by

$$u_N^*(x) = \sum_{|k| \leqslant N} a_k e^{ikx} + \sum_{|k| > N} \frac{A'}{ik} e^{-iky} e^{ikx}, \tag{2.4}$$

where y is an approximation of x_s and A' is an approximation of $[u]_{x_s}$, and

$$a_k = \frac{1}{2\pi} \int_0^{2\pi} u(x)\, e^{-ikx}\, dx.$$

Since the second sum in (2.4) is actually $F(x, y, A') - F_N(x, y, A')$, we have

$$u_N^*(x) = \sum_{|k| \leqslant N} [a_k - \tilde{f}_k(y, A')]\, e^{ikx} + F(x, y, A'). \tag{2.5}$$

Therefore $u_N^*(x)$ defines an approximation in the spectral space $\{e^{ikx}\}_{|k| \leqslant N}$ augmented by sawtooth-like functions $F(x, y, A')$.

The approximation defined in (2.5) yields nonoscillatory numerical results for discontinuous functions, and spectral schemes using this approximation have given high-order accuracy for one-dimensional Euler gas dynamics equations [2, 3]. In order for (2.5) to be nonoscillatory, the approximations for the location of the shock and the magnitude of the shock should be reasonably accurate. Second order accuracy in the location and first order in the magnitude are needed to ensure the uniform nonoscillatory convergence.

In what follows, we present a different method which will be uniformly convergent up to any given order $m > 0$ and, at the same time, retain the spectral accuracy in the smooth regions away from the discontinuities. Furthermore, the requirement of accuracy in shock locations will be much relaxed and computationally robust. Before we discuss the new approximation method we introduce two techniques to be used in our construction. The first one is the essentially non-oscillatory (ENO) polynomial interpolation, and the second is the filtering technique for Fourier approximations.

ENO Polynomial Interpolation

We will follow the notation used in [9]. Let $u(x)$ be a function defined on $I = [0, 2\pi]$ and $\{x_i\}_{i=0}^N$ be the uniform mesh on I, $x_i = ih$, $h = 2\pi/N$. For simplicity of illustration, we assume that $u(x)$ has only one discontinuity at $x_s \in I$. Now given $u(x_i)$, $0 \leqslant i \leqslant N$, define a piecewise mth order polynomial interpolant $Q_m(x; u)$ for $u(x)$ at mesh points x_i, $0 \leqslant i \leqslant N$ as

$$Q_m(x_i; u) = u(x_i) \qquad \text{for} \quad 0 \leqslant i \leqslant N, \tag{2.6}$$

and

$$Q_m(x; u) = q_{m, j+1/2}(x; u) \qquad \text{for} \quad x_j \leqslant x \leqslant x_{j+1}, \tag{2.7}$$

where $q_{m, j+1/2}(x; u)$ is a polynomial of degree m defined below.

Polynomial $q_{m, j+1/2}(x; u)$ interpolates $u(x)$ at $(m+1)$ successive points x_i, $i_m(j) \leqslant i \leqslant i_m(j) + m$. The stencil of these $(m+1)$ mesh points will be chosen according to the smoothness of the data $u(x_i)$ around x_j. A recursive algorithm to define $i_m(j)$ starts by defining

$$i_1(j) = \begin{cases} j & \text{if} \quad x_j \leqslant x_s, \\ j+1 & \text{otherwise,} \end{cases} \tag{2.8}$$

i.e., $q_{1, j+1/2}(x)$ will be the first degree polynomial which interpolates $u(x)$ at x_j, x_{j+1} or x_{j+1}, x_{j+2}. If we assume $q_{k, j+1/2}(x)$ is the kth degree polynomial which interpolates $u(x)$ at

$$x_{i_k(j)}, \ldots, x_{i_k(j)+k}, \tag{2.9}$$

then we need one additional mesh point in order to define $q_{k+1, j+1/2}(x)$. That point may be the nearest one to the left of stencil of (2.9) (i.e., $x_{i_k(j)-1}$) or the nearest one to the right of the stencil of (2.9) (i.e., $x_{i_k(j)+k+1}$). The choice will be based on the absolute values of the corresponding $(k+1)$th order divided differences, namely,

$$i_{k+1}(j) = \begin{cases} i_k(j) - 1 & \text{if} \quad |u[x_{i_k(j)-1}, \ldots, x_{i_k(j)+k}]| \\ & \qquad < |u[x_{i_k(j)}, \ldots, x_{i_k(j)+k+1}]|, \\ i_k(j) & \text{otherwise.} \end{cases} \tag{2.10}$$

The piecewise polynomial $Q_m(x; u)$ defined in (2.6), (2.7) will give uniform nonoscillatory approximations to $u(x)$ up to the discontinuities. In fact it can be shown that

$$\frac{d^k}{dx^k} Q_m(x; u) = \frac{d^k}{dx^k} u(x) + O(h^{m+1-k}) \qquad \text{for} \quad 0 \leqslant k \leqslant m. \tag{2.11}$$

Filtering Techniques for Fourier Approximations

When a function $u(x)$ is discontinuous, its Fourier approximation $u_N(x)$ will be at most first order everywhere [7]. However, there are several ways to recover the loss of the spectral accuracy in the smooth regions of the function $u(x)$ [8, 14]. The most common way is to multiply the Fourier coefficients of $u(x)$ by a decreasing scalar factor σ_k. $|\sigma_k| \to 0$ as $|k| \to N$. Then the resulting series (the filtered approximation) will be denoted by $u_N^\sigma(x)$,

$$u_N^\sigma(x) = \sum_{|k| \leqslant N} \sigma_k a_k e^{ikx}. \tag{2.12}$$

It was proven in [18] that, if σ_k is derived from a scalar function $\sigma(t)$, $0 \leqslant t \leqslant 1$ and $\sigma_k = \sigma(|k|/N)$, $|k| \leqslant N$, and $\sigma(t)$ satisfies the following conditions:

$$\begin{aligned} &\sigma(0) = 1, \\ &\sigma(1) = 0, \\ &\sigma^{(k)}(0) = \sigma^{(k)}(1) = 0 \qquad \text{for} \quad 1 \leqslant k \leqslant K, \end{aligned} \tag{2.13}$$

then $u_N^\sigma(x)$ will converge to $u(x)$ in the smooth regions of $u(x)$ in the order of $O(1/N^{K+1})$. In the actual computations, σ_k is chosen to decay exponentially in terms of the frequency number,

$$\sigma_k = e^{-\alpha(k/N)^{2\ell}} \qquad \text{for} \quad |k| \leqslant N, \tag{2.14}$$

where the constant α is chosen so that σ_N is the machine zero and 2ℓ is called the order of the exponential filtering.

Uniform Spectral Approximations

We now present our new uniform high order non-oscillatory spectral approximations to discontinuous functions. Again, for simplicity, we assume $u(x)$ is a periodic piecewise C^∞ function on $[0, 2\pi]$ with only one discontinuity at x_s. Also we assume that the discontinuity has been detected within an interval $[x_s^l, x_s^r]$.

Let us denote all the mesh points inside the interval $[x_s^l, x_s^r]$ as $x_{i_l}, \ldots, x_{i_r}$. We then define a piecewise mth order polynomial $\varphi(x)$ which interpolates function $u(x)$ at mesh points x_i, $i_l \leqslant i \leqslant i_r$,

$$\varphi(x) = \begin{cases} q_{m,j+1/2}(x) & \text{if} \quad x \in [x_j, x_{j+1}] \\ & \quad \cap [x_s^l, x_s^r] \text{ for some } j, \\ P_l(x) & \text{if} \quad x \in [0, x_s^l], \\ P_r(x) & \text{if} \quad x \in [x_s^r, 2\pi], \end{cases} \tag{2.15}$$

where $q_{m,j+1/2}(x)$ was defined in (2.8)–(2.10) and $P_l(x)$ and $P_r(x)$ are both m'th order polynomials on the interval $[0, x_s^l]$ and $[x_s^r, 2\pi]$ respectively, $m' = 2m+1$, and satisfy the following conditions,

$$\begin{aligned} &P_l^{(k)}(x_s^l) = q_{m,i_l-1/2}^{(k)}(x_s^l), \\ &P_r^{(k)}(x_s^r) = q_{m,i_r+1/2}^{(k)}(x_s^r), \end{aligned} \qquad \text{for} \quad 0 \leqslant k \leqslant m \tag{2.16}$$

and

$$\begin{aligned} &P_l^{(k)}(x_s^r - 2\pi) = q_{m,i_r+1/2}^{(k)}(x_s^r), \\ &P_r^{(k)}(x_s^l + 2\pi) = q_{m,i_l-1/2}^{(k)}(x_s^l). \end{aligned} \qquad \text{for} \quad 0 \leqslant k \leqslant m \tag{2.17}$$

Conditions (2.16) and (2.17) ensure that $\varphi(x)$ will be at least globally C^m continuous. There are exact $2m+2 = m'+1$ constraints on the m'th polynomials $P_l(x)$ and $P_r(x)$, respectively. Therefore they are uniquely defined. By (2.11), the function $\varphi(x)$ will have the following property:

$$\varphi(x_i) = u(x_i) \qquad \text{for} \quad i_l \leqslant i \leqslant i_r, \tag{2.18}$$

$$\varphi(x) - u(x) = O(h^{m+1}) \qquad \text{for} \quad x \in [x_s^l, x_s^r]. \tag{2.19}$$

Next we consider the difference between $u(x)$ and $\varphi(x)$, $v(x) = u(x) - \varphi(x)$. $v(x)$ will be a C^m function everywhere in $[0, 2\pi]$ except at x_s where $[v(x)]_{x_s} = O(h^{m+1})$. Moreover, $v(x_i) = 0$, $i_l \leqslant i \leqslant i_r$. Therefore, the filtered Fourier interpolant $I_N^\sigma v(x)$ will converge to $v(x)$ rapidly,

$$\begin{aligned} v_N^\sigma(x) = I_N^\sigma v(x) &= \sum_{k=-N/2}^{(N/2)-1} \sigma_k \hat{v}_k e^{ikx}, \\ \hat{v}_k &= \frac{1}{N} \sum_{i=0}^{N} (u(x_i) - \varphi(x_i))\, e^{-ikx_i} \\ &= \frac{1}{N} \sum_{i<i_l} (u(x_i) - P_l(x_i))\, e^{-ikx_i} \\ &\quad + \frac{1}{N} \sum_{i>i_r} (u(x_i) - P_r(x_i))\, e^{-ikx_i}, \end{aligned}$$

and σ_k is the filter in (2.14).

Finally we define the uniform spectral approximation $\mathscr{P}u(x)$ of $u(x)$ by

$$\mathscr{P}u(x) = \varphi(x) + v_N^\sigma(x), \qquad \text{for} \quad x \in [0, 2\pi]. \tag{2.20}$$

Then the derivatives of $u(x)$ will be approximated by those of $\mathscr{P}u(x)$, i.e.,

$$\frac{d^k}{dx^k} u(x) \sim \frac{d^k}{dx^k} \mathscr{P}u(x) \qquad \text{for} \quad k > 0. \tag{2.21}$$

To see the accuracy of (2.20) to $u(x)$, let $\rho(x) \in C_0^\infty(x_s^l, x_s^r)$ be a mollifier function with maximum value not greater than one such that

$$\rho(x) = 1 \qquad \text{for } x \text{ near } x_s, \tag{2.22}$$

and

$$v^*(x) = \begin{cases} (1-\rho(x))\, v(x) & \text{if } x \in [x_s^l, x_s^r], \\ v(x) & \text{otherwise.} \end{cases} \tag{2.23}$$

One can easily see that

$$v^*(x_i) = v(x_i) \qquad \text{for } 0 \leqslant i \leqslant N, \tag{2.24}$$

and hence

$$I_N v^*(x) = I_N v(x). \tag{2.25}$$

As $v^*(x) \in C^m(0, 2\pi)$ and is periodic, by standard estimate it can be shown [2] that

$$\|v^*(x) - I_N^\sigma v^*(x)\|_{L_2} \leqslant c \frac{\|v^{*(m)}\|_{L_2}}{N^{m+1}}, \tag{2.26}$$

where c is a constant independent of N.

On the other hand,

$$\begin{aligned} &\|v^*(x) - v(x)\|_{L_2} \\ &\quad = \sqrt{\int_{x_s^l}^{x_s^r} \rho^2(x)\, v^2(x)\, dx} \\ &\quad \leqslant \sqrt{\int_{x_s^l}^{x_s^r} v^2(x)\, dx} \\ &\quad \leqslant \sqrt{\int_{x_s^l}^{x_s^r} (u(x) - \varphi(x))^2\, dx}, \end{aligned} \tag{2.27}$$

by (2.19) we have

$$\|v^*(x) - v(x)\|_{L_2} = O(h^{m+1}). \tag{2.28}$$

It follows from (2.26) and (2.28) that

$$\begin{aligned} \|v(x) - I_N^\sigma v(x)\|_{L_2} &= \|v(x) - I_N^\sigma v^*(x)\|_{L_2} \\ &\leqslant \|v(x) - v^*(x)\|_{L_2} \\ &\quad + \|v^*(x) - I_N^\sigma v^*(x)\|_{L_2} \\ &= O(h^{m+1}). \end{aligned} \tag{2.29}$$

Thus

$$\begin{aligned} &\|\mathscr{P}u(x) - u(x)\|_{L_2} \\ &\quad = \|[\varphi(x) + I_N^\sigma v(x)] - [\varphi(x) + v(x)]\|_{L_2} \\ &\quad = \|v(x) - I_N^\sigma v(x)\|_{L_2} = O(h^{m+1}), \end{aligned} \tag{2.30}$$

which establishes the uniform $(m+1)$th order convergence of the approximation $\mathscr{P}u$ of u in the L_2 norm. Error estimates in a higher order Sobolev norm can be derived similarly.

The spectral convergence of $\mathscr{P}u(x)$ to $u(x)$ in the regions outside $[x_s^l, x_s^r]$ follows from the spectral convergence of $v_N^\sigma(x)$ to $v(x)$ in the smooth regions of $v(x)$.

3. UNIFORM HIGH-ORDER SPECTRAL METHODS

In this section we study uniform high-order spectral methods for conservations laws (1.1). First, we will consider the scalar one-dimensional conservation laws. Extensions to the system of conservation laws and to multi-dimensional problems will be discussed in Section 4.

We will derive the spectral schemes using the method of lines. The time derivative and spatial derivatives will be discretized separately. For simplicity's sake, we use the Euler-forward-difference method for the time derivative and the numerical scheme will be written in the conservative form,

$$u_j^{n+1} = u_j^n - \lambda(\tilde{f}_{j+1/2} - \tilde{f}_{j-1/2}), \tag{3.1}$$

where $u_j^n \sim u(x_j, t_n)$, $x_j = j\,\Delta x$, $t_n = n\,\Delta t$, and Δx and Δt are the spatial mesh size and the time step, respectively; $\lambda = \Delta t/\Delta x$, $\tilde{f}_{j+1/2}$ are the numerical fluxes.

It is observed that if there is a function $h(x)$ such that

$$f(x) = \frac{1}{\Delta x} \int_{x-(\Delta x/2)}^{x+(\Delta x/2)} h(\xi)\, d\xi, \tag{3.2}$$

then

$$f_x(x_j) = \frac{h(x_{j+1/2}) - h(x_{j-1/2})}{\Delta x}. \tag{3.3}$$

This suggests that the numerical fluxes $\tilde{f}_{j+1/2}$ should approximate $h(x_{j+1/2})$ as $\Delta x \to 0$.

We construct $h(x)$ in the same manner as in [17] via its primitive function $H(x)$ modular a linear function,

$$H(x) = \int_{-\Delta x/2}^{x} (h(\xi) - c)\, d\xi, \tag{3.4}$$

where c is a constant chosen so that $H(x)$ will be a periodic function,

$$c = \int_{-\Delta x/2}^{2\pi-(\Delta x/2)} h(\xi)\, d\xi = \Delta x \sum_{j=0}^{N-1} f_j. \tag{3.5}$$

Assuming that (3.2) holds, then

$$\begin{aligned} H(x_{j+1/2}) &= \int_{-\Delta x/2}^{x_{j+1/2}} (h(\xi) - c)\, d\xi \\ &= \sum_{k=0}^{j} \int_{x_{k-1/2}}^{x_{k+1/2}} h(\xi)\, d\xi - c(j+1)\,\Delta x \\ &= \Delta x \sum_{k=0}^{j} f(u(x_k)) - c(j+1)\,\Delta x \\ &\qquad \text{for} \quad 0 \leqslant j \leqslant N. \end{aligned} \tag{3.6}$$

We then form the uniform spectral approximation operator $\mathscr{P}H$ to $H(x)$,

$$\mathscr{P}H = \varphi(x) + v_N^{\sigma}(x), \tag{3.7}$$

where $\varphi(x)$ is the piecewise mth polynomial defined in (2.15) and $v_N^{\sigma}(x)$ is the filtered Fourier interpolant of data $H(x_{j+1/2}) - \varphi(x_{j+1/2})$, $0 \leqslant j \leqslant N$. As before, it is assumed that the shock discontinuity or contact discontinuity x_s (for simpler illustrations, only one such discontinuity is assumed to exist) has been detected in an interval $[x_s^l, x_s^r]$, i.e.,

$$x_s \in [x_s^l, x_s^r]. \tag{3.8}$$

If $x \in [x_j, x_{j+1}] \cap [x_s^l, x_s^r]$ for some j, $\varphi(x) = q_{m,j+1/2}(x)$. $q_{m,j+1/2}(x)$ is an mth order polynomial and

$$\begin{aligned} &q_{m,j+1/2}(x_{j+1/2}) \\ &\quad = H(x_{i+1/2}) \qquad \text{for} \quad i_m(j) \leqslant i \leqslant i_m(j) + m. \end{aligned} \tag{3.9}$$

The stencil $i_m(j), \ldots, i_m(j)+m$ is defined recursively as in (2.8)–(2.10), however, the first point of the stencil $i_1(j)$ is chosen according to the local Roe-speed $a_{j+1/2}$,

$$a_{j+1/2} = \frac{f(u_{j+1}) - f(u_j)}{u_{j+1} - u_j}, \tag{3.10}$$

i.e.,

$$i_1(j) = \begin{cases} j, & \text{if} \quad a_{j+1/2} \geqslant 0, \\ j+1, & \text{if} \quad a_{j+1/2} < 0. \end{cases} \tag{3.11}$$

We then have the following spectral algorithm:

ALGORITHM I (Spectral ENO–Roe).

• Step 1, define $H(x_{j+1/2})$, $0 \leqslant j \leqslant N$ by (3.6) and their uniform spectral approximation $\mathscr{P}H(x)$ by (3.7);

• Step 2, let

$$\begin{aligned} \tilde{f}_{j+1/2} &= \frac{d}{dx}\mathscr{P}H(x_{j+1/2}) + c \\ &= \frac{d}{dx}\varphi(x_{j+1/2}) + \frac{d}{dx} v_N^{\sigma}(x_{j+1/2}) + c, \end{aligned} \tag{3.12}$$

where constant c is defined in (3.5).

Remarks. 1. (Operation counts of the Algorithm.) The traditional plain spectral methods need order of $O(N \log N)$ operations in computing derivatives $f_x(u_j)$, $1 \leqslant j \leqslant N$. The costs of Algorithm I consist of two parts: (1) the computations of the primitive function $H(x_{j+1/2})$, operation counts $N+1$; (2) the computations of derivatives of $\varphi(x_{j+1/2})$ and $v_N(x_{j+1/2})$. Inside the discontinuity interval, $\varphi(x)$ is defined by mth order ENO interpolations, for k cells, the operation counts equal to $3(m*(m+1)/2 + k*m)$ (computation of divided difference tables) $+ 2k(m-1)$ (stencil selection) $+$ $2k*m$ (computation of Newton nested form). As the number of cells inside the discontinuity interval is usually small, about 6–8 cells in all our computations for each discontinuity, so the costs for the ENO interpolation can be ignored. Outside the discontinuity interval, computation of $\varphi_x(x_{j+1/2})$ can be evaluated analytically in $(m+1)*N$ operations where m is the order of polynomial $\varphi(x)$. The evaluation of $(d/dx)\, v_N^{\sigma}(x_{j+1/2})$, $0 \leqslant j \leqslant N$ can be done efficiently via the fast Fourier transformations with the total number of operations of order $O(N \log N)$. Most of the computations except for the ENO part can be well vectorized in current vector machines. The advantage of Algorithm I will be more evident in the case of systems of conservation laws, the characteristic decompositions needed for upwind ENO schemes, thus the ENO interpolations for the characteristic components, only have to be done for those few mesh points inside discontinuity intervals;

2. The formal spatial accuracy of Algorithm I will be spectrally accurate in the smooth regions of the solution and uniformly m-order elsewhere;

3. (Entropy Correction.) The fluxes $\tilde{f}_{j+1/2}$ defined in (3.12) are based on the Roe flux which admits "expansion shocks." In [11], a simple way of entropy correction was suggested for the Roe scheme. For our Algorithm I, we adopt the following entropy corrections. In the cells that contain sonic points, i.e., $f'(u)$ changes signs for $u_j \leqslant u \leqslant u_{j+1}$, we make entropy corrections using the local Lax–Friedrichs fluxes as proposed in [17]. Noting that $\varphi(x_{j+1/2}) = H(x_{j+1/2})$, thus $\varphi[x_{j-1/2}, x_{j+1/2}] = f(u_j) - c$

for $x_j \in [x_s^l, x_s^r]$, therefore we can define a local Lax–Friedrichs flux as in [17]. The resulting fluxes will replace $(d/dx)\,\varphi(x_{j+1/2})$ in Eq. (3.12). The computation of a local Lax–Friedrichs flux costs twice as that of computing an ENO–Roe flux in (3.12), however, it will ensure an entropy-satisfying solution and maintain the formal accuracy of the whole scheme.

4. EULER EQUATIONS OF GAS DYNAMICS

In this section we extend the scalar Algorithm I from the previous section to the system of Euler equations for gas dynamics for polytropic gas. With all variables in boldface denoting vectors, we have the following Euler equations:

$$\mathbf{u}_t + \mathbf{f}(\mathbf{u})_x = 0, \tag{4.1}$$

$$\mathbf{u} = (\rho, m, E)^{\mathrm{T}}, \tag{4.2}$$

$$\mathbf{f}(\mathbf{u}) = q\mathbf{u} + (0, P, qP)^{\mathrm{T}}, \tag{4.3}$$

$$P = (\gamma - 1)(E - \tfrac{1}{2}\rho q^2). \tag{4.4}$$

Here ρ, q, P, and E are the density, velocity, pressure, and total energy, respectively, $m = \rho q$ is the momentum, and $\gamma = 1.4$ is the ratio of specific heats of a polytropic gas.

The eigenvalues of the Jacobian matrix $\mathbf{A}(\mathbf{u}) = \partial \mathbf{f}/\partial \mathbf{u}$ are

$$\lambda_1(\mathbf{u}) = q - c, \qquad \lambda_2(\mathbf{u}) = q, \qquad \lambda_3(\mathbf{u}) = q + c, \tag{4.5}$$

where $c = (\gamma P/\rho)^{1/2}$ is the sound speed.

The corresponding right-eigenvectors are

$$\mathbf{r}_1(\mathbf{u}) = \begin{pmatrix} 1 \\ q - c \\ h - qc \end{pmatrix}, \qquad \mathbf{r}_2(\mathbf{u}) = \begin{pmatrix} 1 \\ q \\ \frac{1}{2}q^2 \end{pmatrix}, \qquad \mathbf{r}_3(\mathbf{u}) = \begin{pmatrix} 1 \\ q + c \\ h + qc \end{pmatrix}, \tag{4.6}$$

where

$$h = (E + P)/\rho = c^2/(\gamma - 1) + \tfrac{1}{2}q^2,$$

is the total enthalpy.

The corresponding left eigenvectors $\{\mathbf{l}_k(\mathbf{u})\}$ which are bi-orthonormal to $\{\mathbf{r}_k(\mathbf{u})\}$ in (4.6) are

$$\begin{aligned} \mathbf{l}_1(\mathbf{u}) &= \tfrac{1}{2}(b_2 + q/c, -b_1 q - 1/c, b_1), \\ \mathbf{l}_2(\mathbf{u}) &= (1 - b_2, b_1 q, -b_1), \\ \mathbf{l}_3(\mathbf{u}) &= \tfrac{1}{2}(b_2 - q/c, -b_1 q + 1/c, b_1), \end{aligned} \tag{4.7}$$

where

$$b_1 = (\gamma - 1)/c^2, \tag{4.8}$$

$$b_2 = \tfrac{1}{2}q^2 b_1. \tag{4.9}$$

As in the case of scalar conservation laws, we first define a vector counterpart $\mathbf{H}(x_{j+1/2})$, $0 \leqslant j \leqslant N$ of (3.6). The scalar quantities $f(u(x_k))$ in (3.6) are replaced by the vectors $\mathbf{f}(\mathbf{u}(x_k))$. We then generalize the construction of the uniform spectral approximation operator $\mathscr{P}\mathbf{H}$ to vector-valued functions in the following way. As before, the assumption about the shock location (3.8) still holds here. We have *the uniform spectral approximation*

$$\mathscr{P}\mathbf{H}(x) = \mathbf{\Phi}(x) + \mathbf{v}_N^{\sigma}(x), \tag{4.10}$$

where the components of the vector-valued function $\mathbf{\Phi}(x)$ will be piecewise mth polynomials and $\mathbf{v}_N^{\sigma}(x)$ will be the filtered Fourier interpolant of vector quantities $\mathbf{H}(x_{j+1/2}) - \mathbf{\Phi}(x_{j+1/2})$, $0 \leqslant j \leqslant N$.

$\mathbf{\Phi}(x)$ will be defined separately according to whether x is inside or outside the interval $[x_s^l, x_s^r]$. For $x \in [x_j, x_{j+1}] \cap [x_s^l, x_s^r]$ for some j, first let $q_{m,j+1/2}^{(k)}(x)$ be the ENO polynomial interpolant of the characteristic variables $\mathbf{H}^{(k)}(x_{i+1/2})$, $j - m \leqslant i \leqslant j + m$. Here as usual the characteristic variables $\mathbf{H}^{(k)}(x_{i+1/2})$ are the projections of $\mathbf{H}(x_{i+1/2})$ on the locally defined characteristic fields. In this paper, we define the local characteristic fields with respect to the Roe-averaged state $\mathbf{u}_{j+1/2}$ between the states $\mathbf{u}_j$, $\mathbf{u}_{j+1}$, i.e.,

$$\mathbf{H}^{(k)}(x_{j+1/2}) = \mathbf{l}_k(\bar{\mathbf{u}}_{j+1/2})\,\mathbf{H}(x_{j+1/2}) \tag{4.11}$$

for $j - m \leqslant i \leqslant j + m$, $1 \leqslant k \leqslant 3$. For the definition of $\bar{\mathbf{u}}_{j+1/2}$, we refer to [15].

So, we have

$$q_{m,j+1/2}^{(k)}(x_{j+1/2}) = \mathbf{H}^{(k)}(x_{j+1/2}) \quad \text{for} \quad i_m(j) \leqslant i \leqslant i_m(j) + m. \tag{4.12}$$

In the recursive process of choosing the stencil $i_m(j)$, the first point $i_1(j)$ is determined according to the sign of the local eigenvalue, specifically

$$i_1(j) = \begin{cases} j & \text{if} \quad \lambda_k(\bar{\mathbf{u}}_{j+1/2}) \geqslant 0, \\ j+1 & \text{if} \quad \lambda_k(\bar{\mathbf{u}}_{j+1/2}) < 0. \end{cases} \tag{4.13}$$

Then we define the vector-valued function $\mathbf{\Phi}(x)$ as

$$\mathbf{\Phi}(x) = \sum_{k=1}^{3} q_{m,j+1/2}^{(k)}(x)\,\mathbf{r}_k(\bar{\mathbf{u}}_{j+1/2}) \quad \text{for} \quad x \in [x_j, x_{j+1}]. \tag{4.14}$$

On the other hand, when x is outside of the interval $[x_s^l, x_s^r]$, we define $\Phi(x)$ in the same way as in (2.16) and (2.17). Therefore, in those regions the components of $\Phi(x)$ will be $m' = (2m+1)$th order polynomials. Globally, the components of $\Phi(x)$ will be C^m function for $x \in [0, 2\pi]$ and

$$\Phi(x_{i+1/2}) = \mathbf{H}(x_{i+1/2}), \qquad \text{if} \quad x_{i+1/2} \in [x_s^l, x_s^r]. \tag{4.15}$$

Now we present out algorithm for (4.1):

ALGORITHM II (Spectral ENO–Roe).

- Step 1, define vector quantities $\mathbf{H}(x_{j+1/2})$, $0 \leqslant j \leqslant N$ by (3.6) and their uniform spectral approximation $\mathscr{P}H(x)$ by (4.10);
- Step 2, let

$$\hat{\mathbf{f}}_{j+1/2} = \frac{d}{dx}\mathscr{P}\mathbf{H}(x_{j+1/2}) + c$$

$$= \frac{d}{dx}\Phi(x_{j+1/2}) + \frac{d}{dx}\mathbf{v}_N^{\sigma}(x_{j+1/2}) + c, \tag{4.16}$$

where c is defined as in (3.5) with f_j replaced by $\mathbf{f}_j$.

Remarks. 1. All of the remarks following Algorithm I of the previous section apply to Algorithm II. However, the entropy correction will be done only on the genuine nonlinear fields. The total number of operations in the computations of all $\hat{\mathbf{f}}_{j+1/2}$, $0 \leqslant j \leqslant N$ will be of order $O(N \log N)$. Moreover, the characteristic decompositions are only needed for those $x_{j+1/2}$ in $[x_s^l, x_s^r]$ where a shock discontinuity or contact discontinuity has been detected;

2. (Generalization to Multi-dimensional cases). For the system of conservation laws in two dimensions (1.1), we apply Algorithm II to $\mathbf{f}(\mathbf{u})$ and $\mathbf{g}(\mathbf{u})$ separately. Characteristic decompositions will be done on their corresponding characteristic fields when needed. The same idea can be applied to higher dimensional cases.

5. NUMERICAL RESULTS

In this section, we will carry out several numerical experiments with Algorithms I and II. In implementing these algorithms, we have to choose the order of ENO interpolations in (3.7) or (4.10) and the interval $[x_s^l, x_s^r]$ as defined in (3.8), which is detected to contain a shock or contact discontinuity. In most of the tests, we choose third-order ENO interpolation, i.e., $m = 3$, unless it is mentioned otherwise. The interval $[x_s^l, x_s^r]$ is usually chosen to contain 6–8 mesh points around a discontinuity. The numerical results show insensitivity to the size of $[x_s^l, x_s^r]$ as long as it contains all transition points in the numerical shock. To detect the shock we have used the basic check on the gradients of the numerical data. Define

$$t_j = \max(|u(j) - u(j-1)|, |u(j+1) - u(j)|). \tag{5.1}$$

If $t_j > \max(3.0t_{j-2}, 3.0t_{j+2}, \alpha)$, where α is chosen dynamically according to the structure of the shock wave, then we decide that the interval $[x_{j-1}, x_{j+1}]$ contains a discontinuity. Because of the global high order of the schemes, a falsely detected shock location in a smooth region of the solution will not destroy the whole accuracy of the scheme (though spectral accuracy will not be retained at those falsely detected discontinuities).

To retain the spectral accuracy in the smooth region of the solutions, we apply high order exponential cut-off filters in (2.14). It is our experience that a very weak filter (i.e., high order) will suffice to get high accuracy in the smooth region.

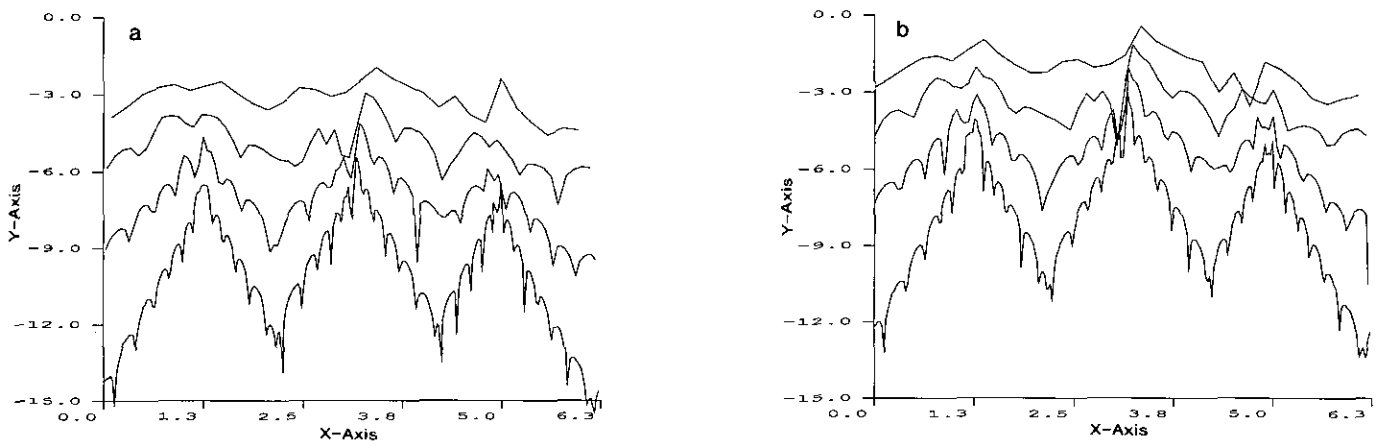

FIG. 1. (a) Uniform spectral approximations to discontinuous funcion, errors in function values on the logarithm scale, $N = 32$, 64, 128, and 256; (b) error in first derivative values on the logarithm scale, $N = 32$, 64, 128, and 256.

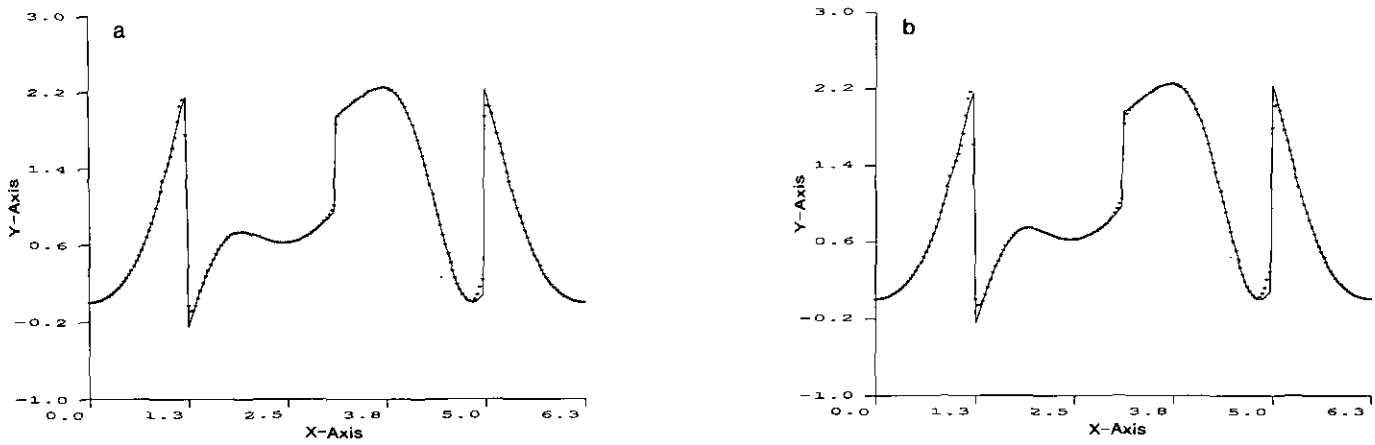

FIG. 2. Linear advection of discontinuous solutions with subcell resolutions, $N = 200$; (a) time $t = 2\pi$ and (b) time $t = 4\pi$.

Time Discretization for Chebyshev Methods

The time derivative in (4.1) is discretized with the Runge–Kutta method. We have used the third order Runge–Kutta method proposed in [17] which yields TVD (total variation vanishing) results if the spatial discretization is TVD.

For periodic problems, the spatial derivative is approximated by Fourier trigonometric polynomials. When the solution is nonperiodic, Chebyshev polynomials are used instead. A common difficulty, however, with Chebyshev methods is the stringent time-step restriction. In general, the time step Δt has to be in the order of $O(1/N^2)$, where N is the order of the Chebyshev polynomials. As in most orthogonal polynomial based collocation method, the collocation points are clustered near the solution boundaries. For the test problems in this paper, this dense distribution of mesh points near boundaries is not necessary. Recently in [12], a novel mesh transformation is proposed to relax the restriction of the Chebyshev methods on time steps. If x denotes the physical coordinate and ξ the computational coordinate, the following transformation is considered in [12]:

$$\xi = \frac{\sin^{-1} \alpha x}{\sin^{-1} \alpha} \qquad |x| \leqslant 1,\ |\xi| \leqslant 1. \tag{5.2}$$

If $\xi_i = \cos i(\pi/N)$, $0 \leqslant i \leqslant N$ is the Chebyshev mesh in the ξ-space, then $x_i = (1/\alpha)\ \sin(\sin^{-1}\alpha\xi_i)$ will be the corresponding mesh in the x-space. Because of the stretching nature of the transformation (5.2), mesh points x_i will be more uniformly distributed in the physical x-space. A Chebyshev polynomial in the transformed ξ-space will be used to approximate the derivative with respect to ξ, and the derivative with respect to x will be computed as follows:

$$\frac{d}{dx} = \frac{d}{d\xi}\frac{d\xi}{dx} = \frac{\alpha}{\sin^{-1}\alpha \cos(\sin^{-1}\alpha\xi)}\frac{d}{d\xi}. \tag{5.3}$$

In our computations, we have observed an improvement

TABLE I

Global L_1 Error and L_1 Error in the Smooth Region for the Burgers' Equations at Time $t = 2$; the Smooth Region Is Defined to be 0.8 Away from the Shock Location

N	Global	Order	Smooth region	Order
32				
	1.49(−4)		1.17(−4)	
64		2.5		4.3
	2.70(−5)		5.86(−6)	
128		2.9		6.5
	3.70(−6)		6.54(−8)	
256		3.7		10.0
	2.95(−7)		6.36(−11)	

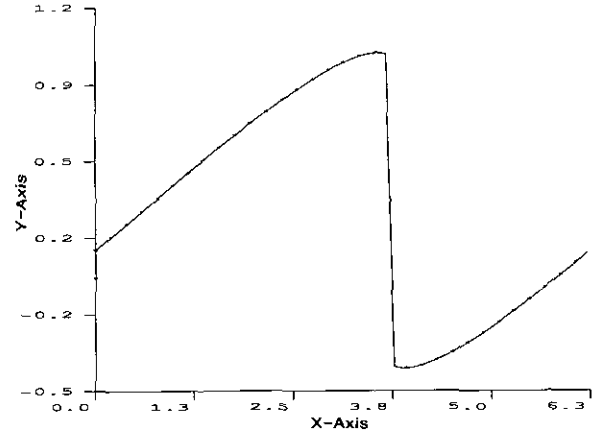

FIG. 3. Solutions to the inviscid Burgers' equation with Algorithm I, $N = 32$, $t = 2$: Numerical solutions (plus), exact solutions (solid lines).

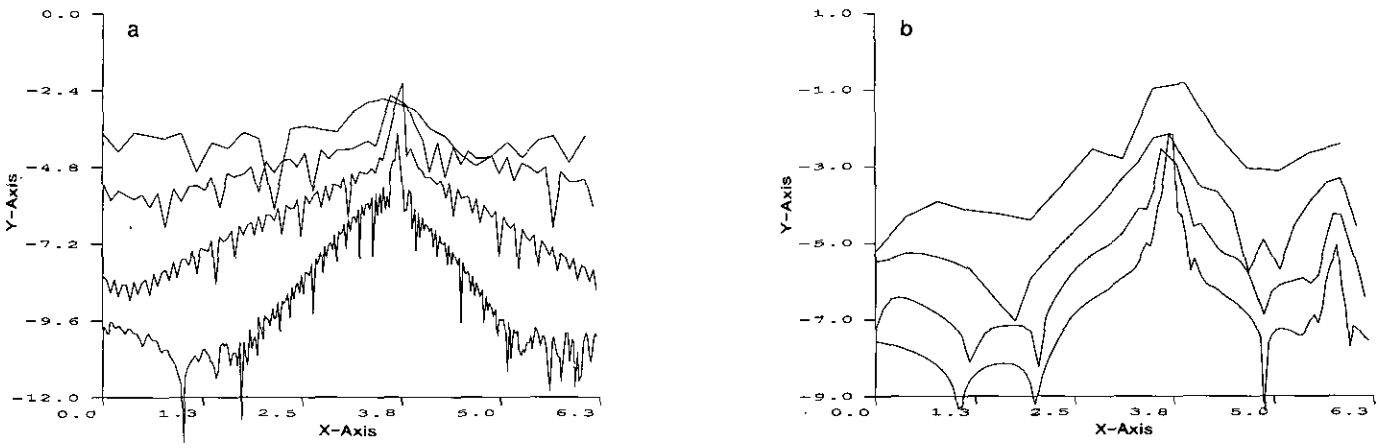

FIG. 4. Errors to the inviscid burgers' equations for $N = 32, 64, 128$, and 256 at time $t = 2$: (a) the spectral Algorithm I and (b) the third-order ENO finite difference methods.

of one magnitude in the time step with $\alpha = 0.999$; at the same time, the resolution of the numerical method is also enhanced in the interior of the physical domain. We refer the reader to [12] for more details about the evaluation of the transformation.

Uniform Spectral Approximation for Discontinuous Functions. We consider the following piecewise C^∞ function:

$$g(x) = e^{\sin^2 x} \begin{cases} -\sin(2(x+0.7\pi)) + 1 & -\pi \leqslant x \leqslant -\frac{2}{5}\pi, \\ \sin^2 x & |x| \leqslant \frac{2}{5}\pi, \\ \frac{2}{\pi}x - 1 - \frac{\sin 3x}{6} & \frac{2}{5}\pi < x \leqslant \pi. \end{cases} \tag{5.4}$$

$g(x)$ is extended periodically outside of $[-\pi, \pi]$, thus $g(x)$ has three discontinuities in the interval $[0, 2\pi]$. The profile of $g(x)$ is plotted as the solid line in Fig. 2. Given the mesh value $g(x_i)$, $x_i = 2\pi i/N$, $0 \leqslant i \leqslant N$, we use (2.20) and (2.21) to approximate $g(x_{j+1/2})$ and $(d/dx)\, g(x_j)$, $0 \leqslant j \leqslant N$, respectively. In Figs. 1a and 1b, we plot the errors in function values and first derivative values respectively on a logarithm scale for different N's, i.e., $N = 32, 64, 128, 256$. In all of the runs, a 16th order of exponential cut-off filter is used and the third order of ENO interpolation in (2.15) is used. We clearly see the uniform convergence and spectral accuracy in the smooth parts of the function $g(x)$.

Linear Advection of Discontinuous Solution with Subcell Resolution. In order to reduce the smearing in contact discontinuities by shock capturing schemes, Harten [10] suggested a subcell resolution technique to treat one-dimensional contact discontinuities in the context of the cell-averaged ENO finite difference schemes. Later on, this idea was extended to the point-value version of the ENO finite difference scheme in [17]. We test the subcell resolution by our spectral methods.

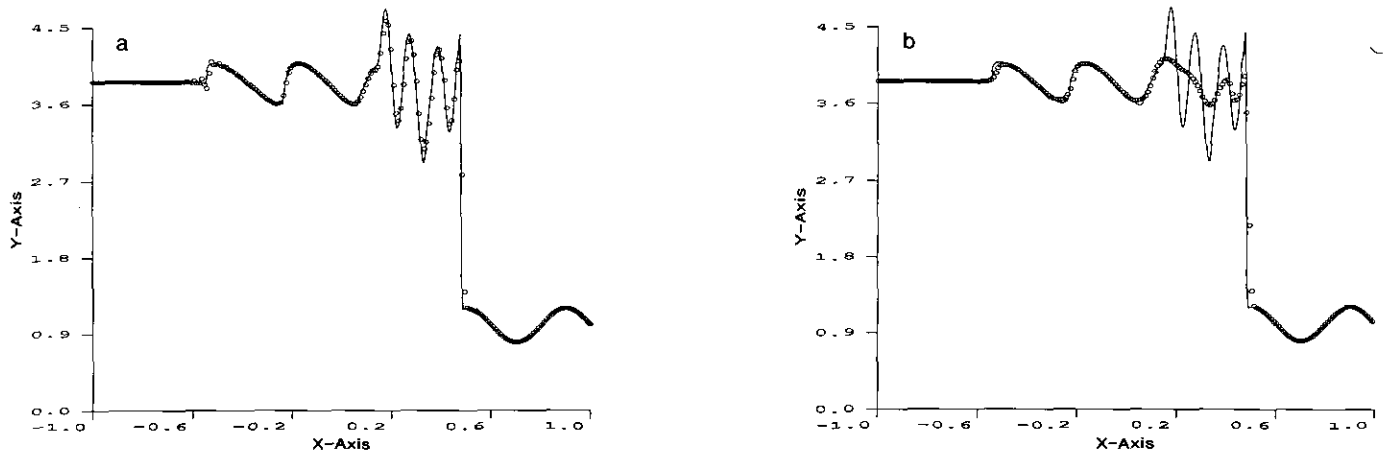

FIG. 5. Interactions between one-dimensional shock wave and density waves with $N = 200$ at time $t = 0.36$: (a) the spectral Algorithm I and (b) the second-order MUSCL schemes.

Consider the initial boundary value problem of the following linear hyperbolic equation,

$$\begin{aligned} u_t &= u_x, \\ u(x, 0) &= g(x), \qquad x \in [0, 2\pi], \\ u(0, t) &= u(2\pi, t) \end{aligned} \tag{5.5}$$

where $g(x)$ is defined in (5.4).

In Figs. 2a and 2b, we plot the numerical solution for $N = 200$ after one and two cycles, i.e., $t = 2\pi$, $t = 4\pi$. In both runs, we have used the 10th order exponential cut-off filters.

Inviscid Burgers' Equation. In this classic example of shock wave computation, we consider the initial value problem with sine wave initial conditions,

$$\begin{aligned} u_t + \left(\frac{u^2}{2}\right)_x &= 0, \\ u(x, 0) &= \alpha + \beta \sin x \qquad x \in [0, 2\pi], \\ u(0, t) &= u(2\pi, t), \end{aligned} \tag{5.6}$$

where $\alpha = 0.3$, $\beta = 0.7$.

The solution to (5.6) develops a shock discontinuity at time $t = 1/\beta$. When $\alpha \neq 0$, the solution consists of a moving shock wave after $t = 1/\beta$. As the exact solution for this problem can be obtained by iterative methods, we use this example to test the global accuracy of the scalar Algorithm I with $m = 3$ (i.e., the third order of ENO interpolation is used in (3.7)). In Table I, we list the global L_1 error of the numerical solutions and the L_1 error in the smooth region of the solution at time $t = 2$ and $N = 32$, 64, 128, and 256. In computing the global L_1 error, we exclude the occasional one transition point across the shock, and for the L_1 error in smooth region, we exclude a neighborhood with radius 0.8 centered at the shock location. The third column of Table I shows the global third-order accuracy in L_1 norm of Algorithm I, and the fifth column shows the increasing order of accuracy in the smooth region. In all of the runs, the time step has been chosen such that further decreasing of the time step does not improve the final accuracy. Therefore, the dominant errors come from the spatial discretization. In Fig. 3, solutions at time $t = 2$ and $N = 32$ are plotted (plus) against the exact solution (solid lines). In Fig. 4a, the errors for $N = 32$, 64, 128, and 256 at time $t = 2$ are plotted

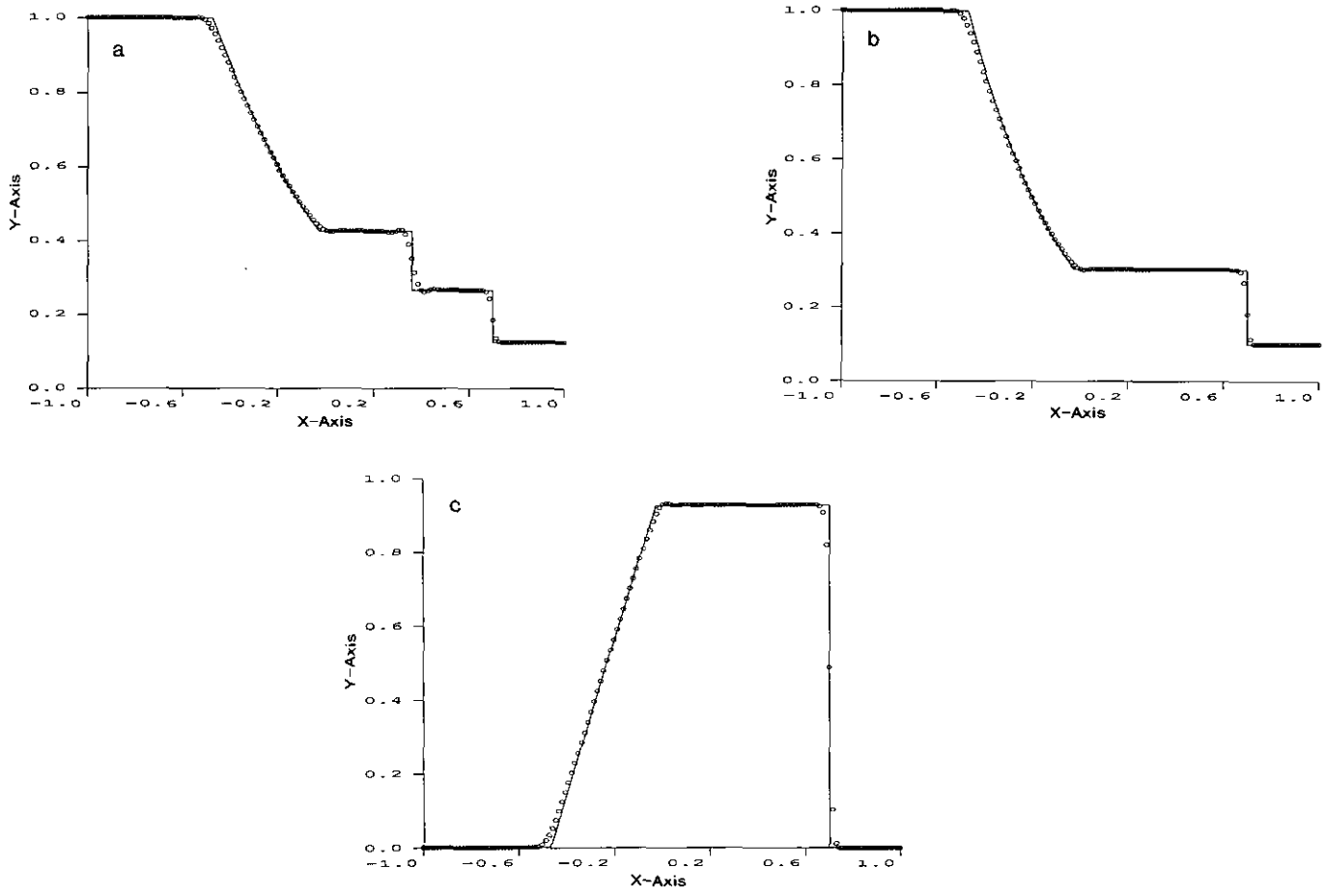

FIG. 6. Solutions of Sod's problem with $N = 150$ at time $t = 0.4$: (a) density, (b) velocity, and (c) pressure.

in logarithm scale. For a comparison, we plot the errors with the same parameters for the third-order ENO finite difference scheme in Fig. 4b.

One-Dimensional Euler Gas Dynamics Equations. We solve the system of equations (4.1) with different initial data.

(1) Interaction of a shock wave and density waves:

We consider the following initial condition for (4.1),

$$\begin{aligned} &\rho_l = 3.857143,\ q_l = 2.629367,\ P_l = 10.333333 \\ &\qquad -1 \leqslant x \leqslant -0.8, \\ &\rho_r = 1 + \varepsilon \sin 5\pi x,\ q_r = 0,\ P_r = 1 \\ &\qquad -0.8 < x \leqslant 1, \end{aligned} \tag{5.7}$$

where $\varepsilon = 0.2$.

In Algorithm II, we choose the third-order ENO interpolation and the 16th order exponential cut-off filters. In Fig. 5a, we display the density profile for $N = 200$ at $t = 0.36$, the solid lines are the solutions obtained by the third order ENO finite difference methods with 800 points. For a comparison, we plot the solution obtained with the second order MUSCL schemes with $N = 200$ in Fig. 5b.

(2) Sod's problem and Lax' problem:

We now consider the standard Riemann problem of (4.1) with the following initial data [16];

(a) Sod's problem

$$\begin{aligned} &(\rho_l, q_l, P_l) = (1, 0, 1) && -1 \leqslant x \leqslant 0, \\ &(\rho_r, q_r, P_r) = (0.125, 0, 0.10) && 0 \leqslant x \leqslant 1; \end{aligned}$$

(b) Lax's problem:

$$\begin{aligned} &(\rho_l, q_l, P_l) = (0.445, 0.698, 3.528) && -1 \leqslant x \leqslant 0, \\ &(\rho_r, q_r, P_r) = (0.5, 0, 0.571) && 0 \leqslant x \leqslant 1. \end{aligned}$$

For Lax's problem, the subcell resolution has been applied on the linear degenerated field near contact discontinuities. In both of the problems, we use the third-order

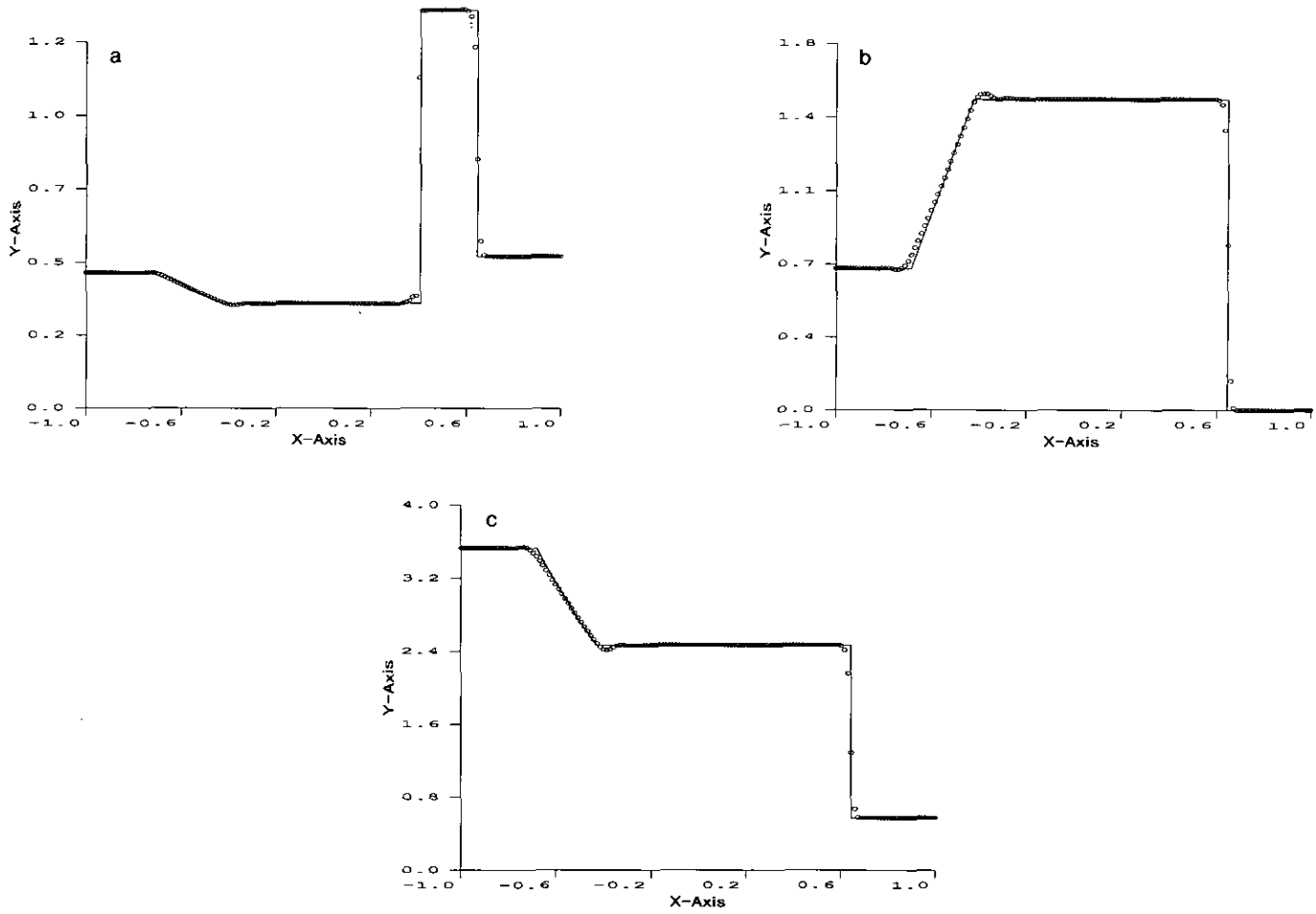

FIG. 7. Solutions of Lax's problem with $N = 150$ at time $t = 0.26$: (a) density, (b) velocity, and (c) pressure.

ENO interpolation in Algorithm II and the 10th order exponential cut-off filters. In Figs. 6a–6c the solutions of the Sod's problems with $N=150$ at time $t=0.4$ are plotted, while Figs. 7a–7c display the solutions of the Lax's problem with $N=150$ at time $t=0.26$. In both cases, the solid lines are the exact solutions.

Interaction of Blast Waves. The initial data suggested in [20] to simulate the interactions of two blast waves is

$$\mathbf{u}(x,0)=\begin{cases}\mathbf{u}_L & 0\leqslant x\leqslant 0.1,\\ \mathbf{u}_M & 0.1\leqslant x\leqslant 0.9,\\ \mathbf{u}_R & 0.9\leqslant x\leqslant 1,\end{cases} \tag{5.8}$$

where $\rho_L=\rho_M=\rho_R=1$, $q_L=q_M=q_R=0$, $P_L=10^3$, $P_M=10^{-2}$, $P_R=10^2$.

The solution to this problem possesses drastic fluctuations under the impact of interactions; it is a good test of the stability of Algorithm II. The complex structure of the solutions after the clash of two blast waves demands a stable high-order method to capture the details of solutions. Unlike the finite difference methods, the spectral methods do not require exterior mesh points to treat boundary conditions. We apply characteristic boundary conditions on both boundaries. As the boundaries are treated as solid walls, we impose the condition that velocity variables vanish on both boundaries, i.e., $q_0=0$, $q_N=0$.

In Figs. 8a–8c and Figs. 9a–9c, we plot the state variables with $N=300$ at time $t=0.028$ and $t=0.038$, respectively. The former is an instant before the clash and the latter is one after the clash. The solid lines in both Figs. 8 and 9 are the solutions obtained with the third-order ENO finite difference methods with 800 mesh points. In Fig. 10, the solutions of density with $N=400$ are also plotted.

Interaction between a Two-Dimensional Shock Wave and a Rotating Vortex. The equations in consideration will be (1.1) with

$$\mathbf{u}=(\rho, m_x, m_y, E), \tag{5.9}$$

$$\mathbf{f}(\mathbf{u})=q_x\mathbf{u}+(0, P, 0, q_xP), \tag{5.10}$$

$$\mathbf{g}(\mathbf{u})=q_y\mathbf{u}+(0, 0, P, q_yP), \tag{5.11}$$

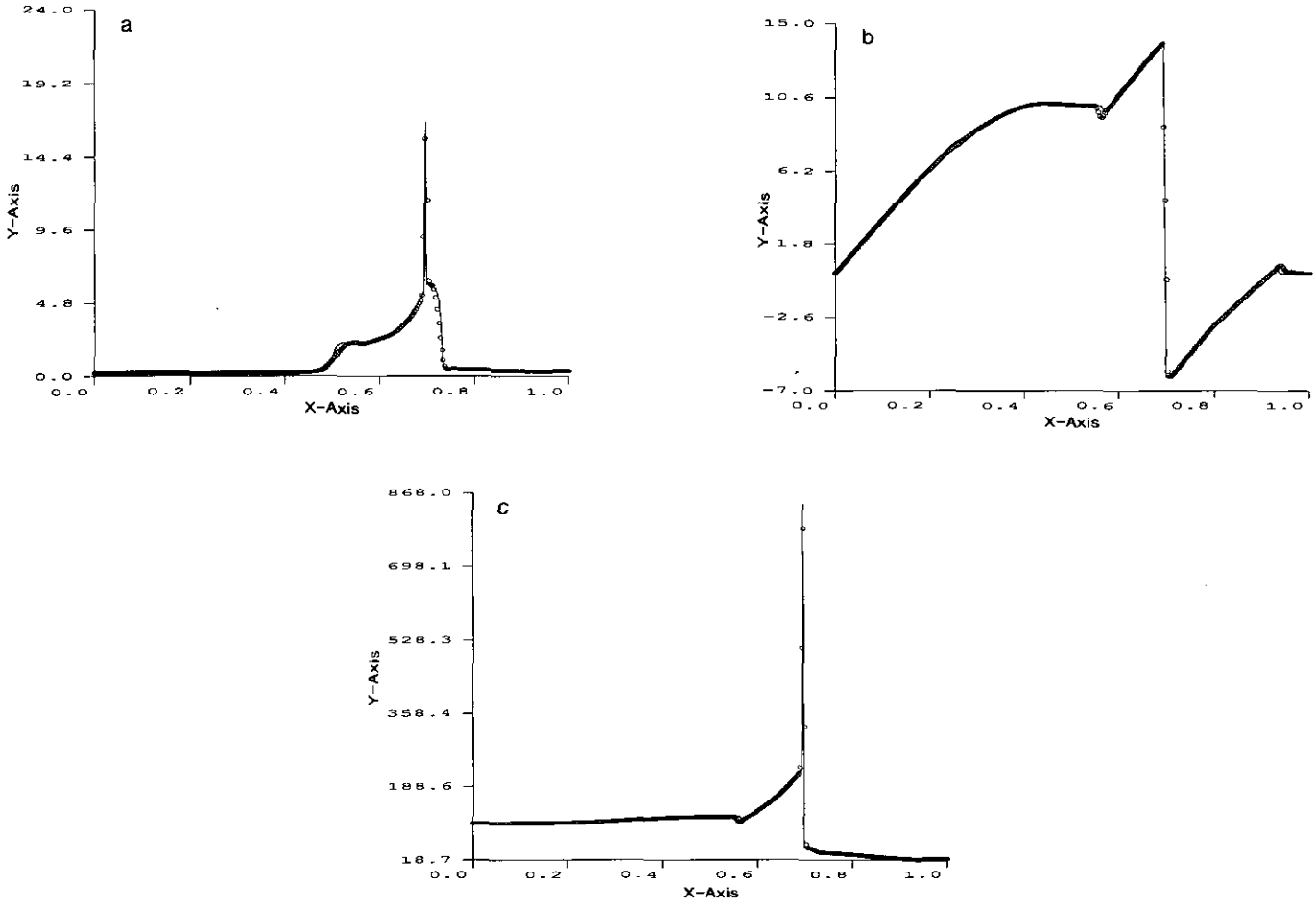

FIG. 8. Blast wave problem with $N=300$ at time $t=0.028$: (a) density, (b) velocity, and (c) pressure.

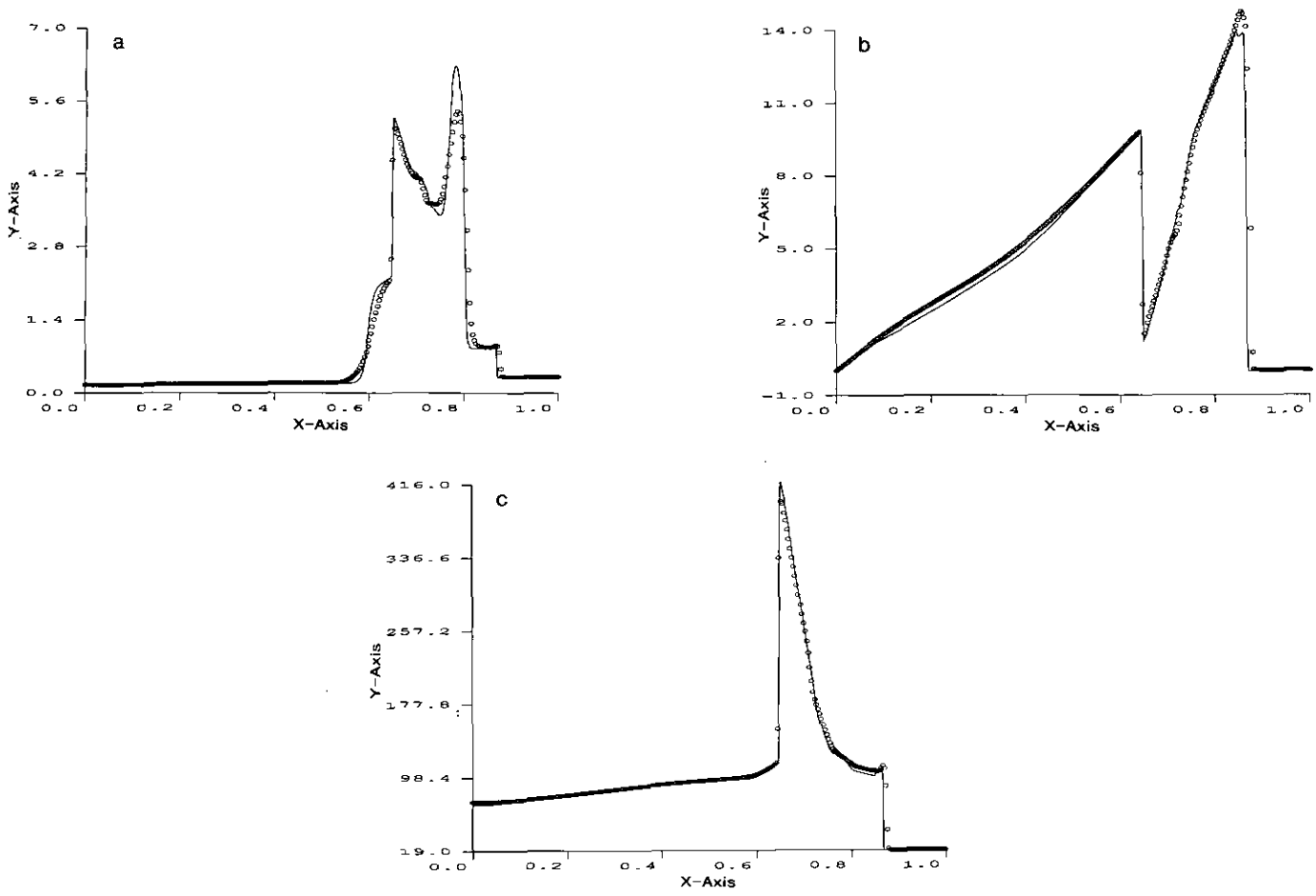

FIG. 9. Blast wave problem, time $t = 0.038$.

where q_x, q_y are velocity components in the x- and y-directions, respectively, and $m_x = \rho q_x$ and $m_y = \rho q_y$ are x- and y-momentums, respectively. $P = (\gamma - 1)(E - \frac{1}{2}\rho q^2)$, $q^2 = q_x^2 + q_y^2$.

We apply the one-dimensional Algorithm II on the fluxes $\mathbf{f}(\mathbf{u})$ and $\mathbf{g}(\mathbf{u})$ separately. The right and left eigenvectors for the Jacobian matrices $(\partial \mathbf{f}/\partial \mathbf{u})$, $(\partial \mathbf{g}/\partial \mathbf{u})$ can be found in [15].

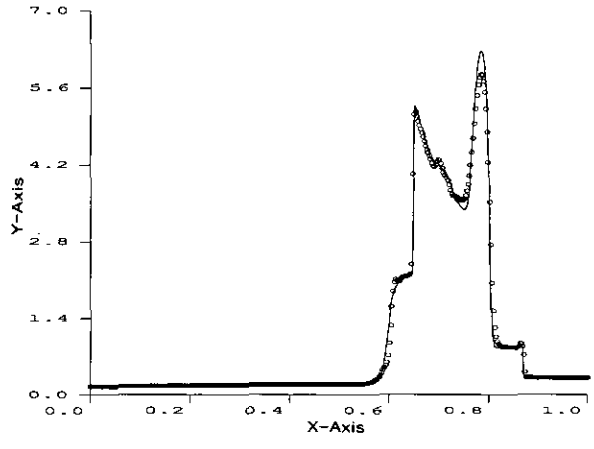

FIG. 10. Density of blast wave problem with $N = 400$ at time $t = 0.038$.

The physical domain is the rectangle $[0, 3] \times [-1.5, 1.5]$. A Mach-3 planar shock wave moves from the left to the right. A rotating vortex is initially located to the right of the shock. As time progresses, the shock will hit the vortex and interact with it. The shock front will be deformed by the interaction, and pressure waves are generated from the interactions. In the computations, we define the velocity fields of the vortex as those induced by two rotating concentric cylinders with radius r_1 and r_2, respectively, $r_1 < r_2$. Initially the vortex is located at (x_c, y_c). The outside cylinder is stationary and the inside one rotates with the angular velocity ω. Let $\tilde{v}(r)$ be the radius velocity at a distance r from the center of the vortex, we then have

$$\tilde{v}(r) = \begin{cases} \omega r & \text{if } 0 \leqslant r \leqslant r_1, \\ \omega \dfrac{1}{r}\left(\dfrac{1}{ra} + \dfrac{r r_1^2}{b}\right) & \text{if } r_1 \leqslant r \leqslant r_2, \\ 0 & \text{if } r \geqslant r_2, \end{cases} \tag{5.12}$$

where $a = 1/r_1^2 - 1/r_2^2$, $b = r_1^2 - r_2^2$, $r = \sqrt{(x - x_c)^2 + (y - y_c)^2}$. We choose $r_1 = 0.15$, $r_2 = 0.75$, $\omega = 7.5$.

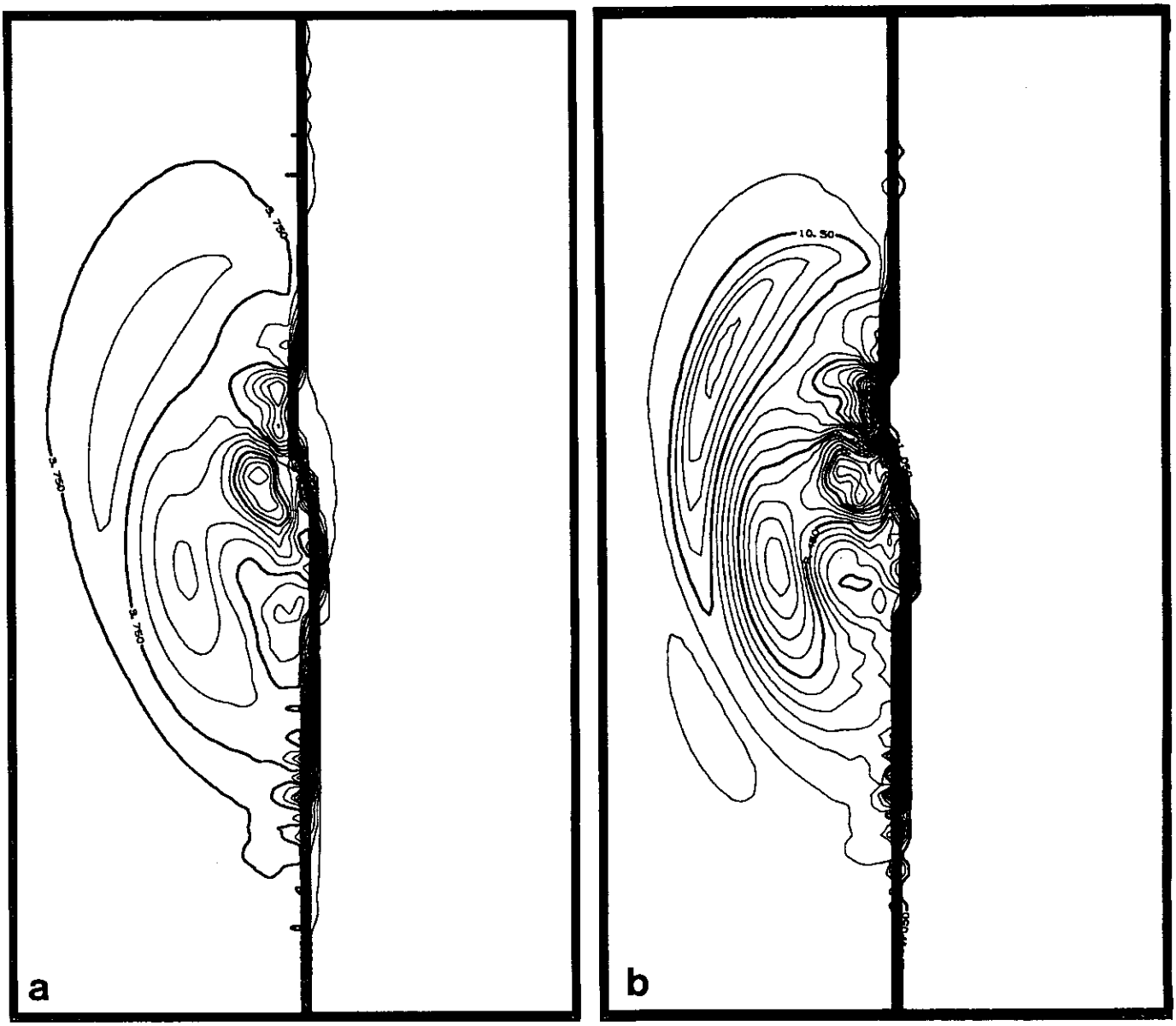

FIG. 11. Interactions between a two-dimensional planner shock wave and a vortex, Mach number = 3, $t = 0.4$: (a) density contour with level value = 0.1 and (b) pressure contour with level value = 0.2.

Therefore the x- and y-velocities induced by this vortex at (x, y) will be

$$\tilde{q}_x = -\frac{y - y_c}{r}\tilde{v}(r), \tag{5.13}$$

$$\tilde{q}_y = \frac{x - x_c}{r}\tilde{v}(r), \tag{5.14}$$

where $x_c = 2.25$, $y_c = 0$.

The initial conditions for the simulation are as follows:

$$\rho_l = 3.857143,$$

$$q_{xl} = 2.629367 \quad \text{if} \quad x < x_0,$$

$$q_{yl} = 0, \tag{5.15}$$

$$P_l = 10.333333, \tag{5.16}$$

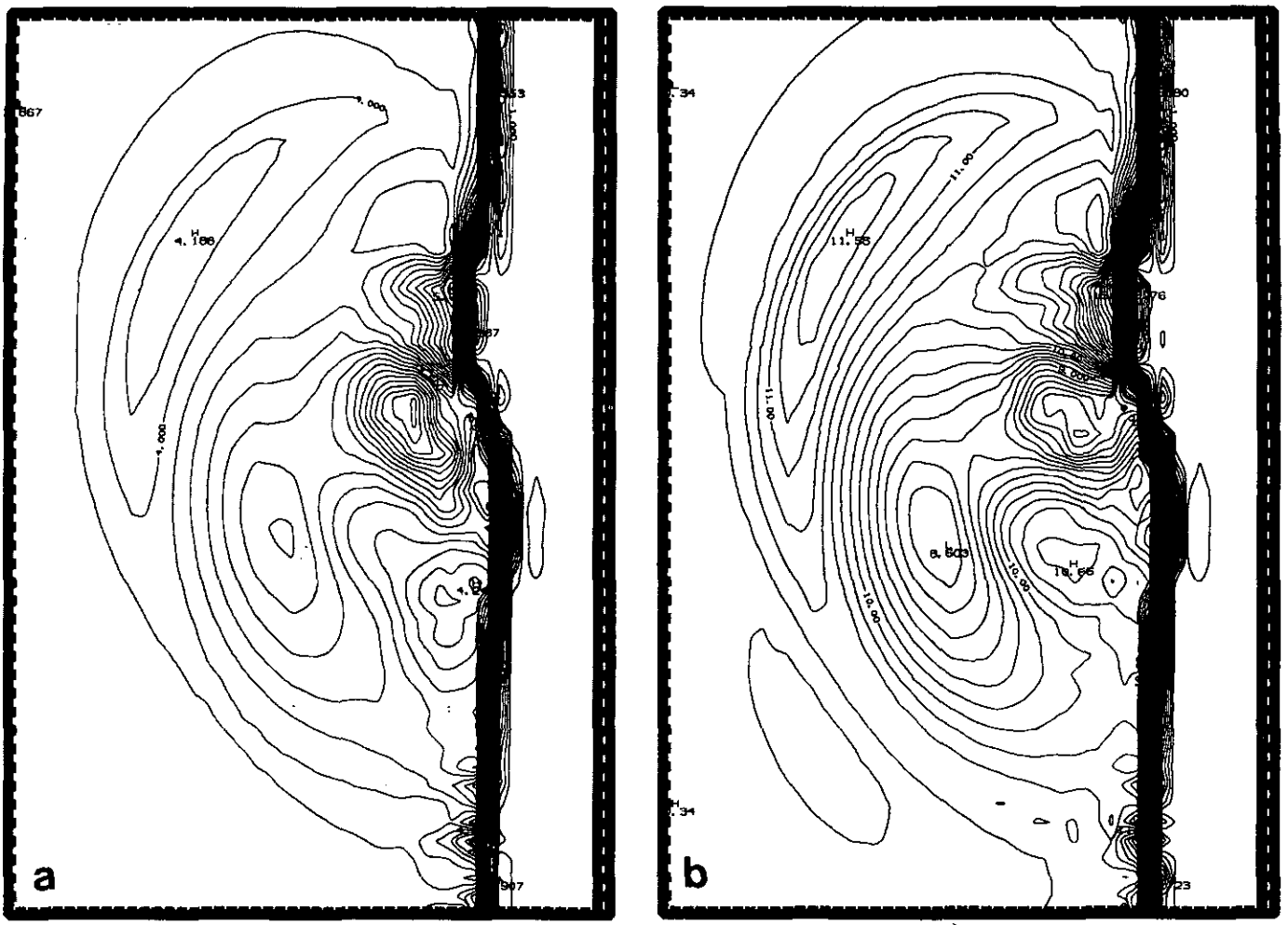

FIG. 12. Close-ups of Fig. 11: (a) density and (b) pressure.

and

$$\begin{aligned} \rho_r &= 1, \\ q_{xr} &= \tilde{q}_x \quad \text{if} \quad x > x_0, \\ q_{yr} &= \tilde{q}_y, \\ P_r &= 1, \end{aligned} \tag{5.17}$$

where x_0 is the initial shock position, $x_0 = 1.5$.

We impose characteristic boundary conditions on both the left and right boundaries. A periodic boundary condition is used in the y-direction and hence we are simulating the interaction between an array of periodically distributed vortices and a plane shock wave. To relax the time restrictions of the Chebyshev approximation in the x-direction, we apply the mesh transformation (5.2) with $\alpha = 0.999$. The shock has been made stationary by a translation in the mean flow direction. The second-order ENO interpolation and the 10th order exponential filter have been used in (4.10).

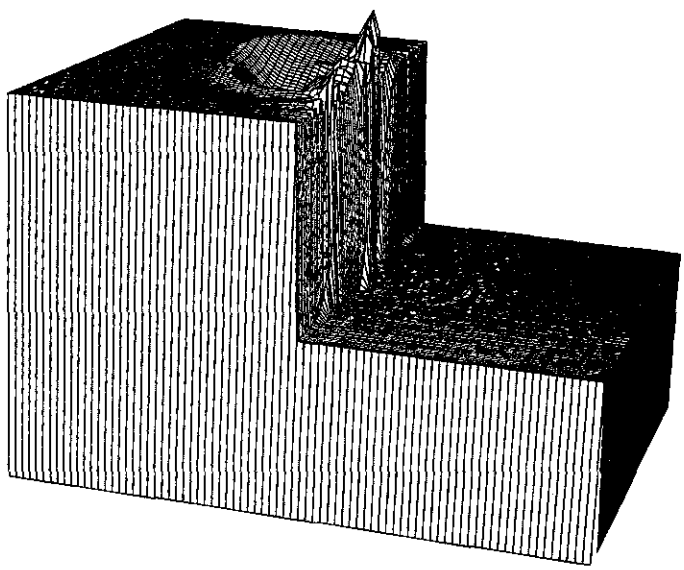

FIG. 13. Same as in Fig. 11, density solutions at $t = 0.4$.

Figures 11a and 11b are the contour plots of the pressure and density fields at time $t = 0.4$, while Figs. 12a, 12b are the close-ups of the pressure and density at time $t = 0.4$. Figure 13 is the pressure profile at time $t = 0.4$.

Concluding Remarks

Centered difference methods including spectral methods are efficient and accurate, while upwind difference methods offer the advantages of sharp monotonic shock profiles. We have explored, in this work, the possibilities of blending the advantages of the ENO finite difference methods and the spectral methods. Numerical results have shown the robustness and feasibility of this approach at a small extra cost over the standard spectral methods. The success of the method proposed in this paper to achieve uniform high-order accuracy is closely related to the ability of the algorithm in detecting shock, contact, and rarefaction discontinuities in the solutions. Future numerical experiments will be concentrated on more efficient techniques in detecting those discontinuities, especially discontinuities in solution deivatives.

ACKNOWLEDGMENTS

We thank Professor David Gottlieb for many useful discussions and also Dr. Waison Don for suggestions on several computational issues. We also express our thanks to the reviewers' careful suggestions.

REFERENCES

1. J. P. Boris, and D. L. Book, *J. Comput. Phys.* **11**, 38 (1973).
2. Wei Cai, *Essentially Non-oscillatory Spectral Methods for Shock Wave Computations*, Ph.D. Thesis, Brown University, Division of Applied Mathematics, Providence, RI, (1989).
3. W. Cai, D. Gottlieb, and A. Harten, *Comput. Math. Appl.* **24**, No. 5/6, 37 (1992).
4. W. Cai, D. Gottlieb, and C. W. Shu, *Math. Comput.* **52** (186), 389 (1989).
5. C. Canuto, M. Y. Hussaini, A. Quarternoni, and T. A. Zang, *Spectral Methods in Fluid Dynamics* (Springer-Verlag, Berlin/New York, 1988).
6. B. Engquist, P. Lotstedt, and B. Sjogreen, *Math. Comput.* **52**, 509 (1989).
7. D. Gottlieb and S. Orzarg, *Numerical Analysis of Spectral Methods: Theory and Applications* (SIAM-CBMS, Philadelphia, 1977).
8. D. Gottlieb and E. Tadmor, Recovering pointwise values of discontinuous data within spectral accuracy, in *Progress and Supercomputing in Computational Fluid Dynamics*, edited by E. M. Murman and S. S. Abarbanel (Birkhäuser, Boston, 1985), p. 357.
9. A. Harten, B. Engquist, S. Osher, and S. Chakravarthy, *J. Comput. Phys.* **71**, 231 (1987).
10. A. Harten, "ENO Schemes with Subcell Resolutions," Icase Report No. 87-56 (August 1987).
11. A. Harten and J. M. Hyman, *J. Comput. Phys.* **50**, 235 (1983).
12. D. Kosloff and Tal-Ezer Hillel, Modified Chebyshev pseudo-spectral method with $O(1/N)$ time step restriction, Icase Report No. 89-71 (December, 1989).
13. F. Lafon and S. Osher, "High Order Filtering Methods for Approximating Hyperbolic Systems of Conservation Laws," Icase Report No. 90-25 (March, 1990).
14. A. Majda, J. McDonough, S. Osher, *Math. Comput.* **32**, 1041 (1978).
15. P. Roe, *J. Comput. Phys.* **43**, 357 (1981).
16. G. A. Sod, *J. Comput. Phys.* **27**, 1 (1978).
17. C.-W. Shu and S. Osher, *J. Comput. Phys.* **83**, 32 (1989).
18. H. Vandeven, "Family of Spectral Filters for Discontinuous Problems," Preprint of Centre De Mathematiques Appliquees (Unite de Recherche Associee au CNRS - 756), Ecole Polytechnique, France (April, 1987).
19. B. van Leer, *J. Comput. Phys.* **32**, 101 (1979).
20. P. Woodward and P. Colella, *J. Comput. Phys.* **54**, 115 (1984).